



Contents lists available at ScienceDirect

Journal of King Saud University – Science

journal homepage: www.sciencedirect.com



Original article

# Molecular structure simulation of (*E*)-2-(butan-2-ylidene)hydrazinecarbothioamide using the DFT approach, and antioxidant potential assessment of its complexes

Tahmeena Khan<sup>a,\*</sup>, Iqbal Azad<sup>a</sup>, Rumana Ahmad<sup>b</sup>, Alfred J. Lawrence<sup>c</sup>, Mohammad Azam<sup>d</sup>, Saikh Mohammad Wabaidur<sup>d</sup>, Saud I. Al-Resayes<sup>d</sup>, Saman Raza<sup>c</sup>, Abdul Rahman Khan<sup>a</sup><sup>a</sup> Department of Chemistry, Integral University, Dasauli, P.O. Bas-ha, Kursi Road, Lucknow 226026, UP, India<sup>b</sup> Department of Biochemistry, Era's Lucknow Medical College and Hospital, Era's University, Lucknow 226003, U.P., India<sup>c</sup> Department of Chemistry, Isabella Thoburn College, 7, Faizabad Road, Lucknow 226007, UP, India<sup>d</sup> Department of Chemistry, College of Science, King Saud University, PO Box-2455, Riyadh 11451, Saudi Arabia

## ARTICLE INFO

### Article history:

Received 15 November 2020

Revised 10 December 2020

Accepted 17 December 2020

Available online 24 December 2020

### Keywords:

Gaussian

Optimization

Quantum

Mechanics

Thiosemicarbazone

Antioxidant

## ABSTRACT

The molecular structure of (*E*)-2-(butan-2-ylidene)hydrazinecarbothioamide (2-butanone thiosemicarbazone) was validated by density functional theory (DFT) calculations. The characterization of the ligand was done using various spectroscopic techniques. Four transition metal complexes were prepared with the ligand and their antioxidant activity was tested. Molecular docking studies of the complexes were also performed against nicotinamide adenine dinucleotide phosphate (NADPH) and myeloperoxidase (MPO). Structure validation of the ligand was done in Gaussian 09 software. The geometry optimization was done at B3LYP/6-31G++(d,p) level. The <sup>1</sup>H and <sup>13</sup>C NMR chemical shifts, FT-IR vibrations and UV-visible transitions were validated with the help of theoretical calculations. The frontier molecular orbital analysis, molecular electrostatic potential (MEP) and global reactivity descriptors were calculated to predict the stability of the molecule. Non-linear optical (NLO) properties were assessed and compared with urea. Natural bond orbital (NBO) analysis was done to predict the stability of the ligand resulting from hyper conjugative interactions and electron delocalization. Molecular docking studies of the complexes were performed with iGEMDOCK 2.1 and AutoDock 4.2.6. Antioxidant potential was assessed by 2,2-diphenyl-1-picrylhydrazyl (DPPH) Assay. <sup>1</sup>H and <sup>13</sup>C correlation coefficients (R<sup>2</sup>) were 0.9964 and 0.9974 respectively. In case of FT-IR, the correlation coefficient (R<sup>2</sup>) was 0.9984. [Fe(C<sub>5</sub>H<sub>11</sub>N<sub>3</sub>S)<sub>2</sub>(SO<sub>4</sub>)] possessed maximum antioxidant potential followed by [Cu(C<sub>5</sub>H<sub>11</sub>N<sub>3</sub>S)<sub>2</sub>(SO<sub>4</sub>)]. Molecular docking findings suggested that the Fe complex released the minimum binding energy. Computational structure validation is an important aspect in finding a lead moiety. The theoretical spectral findings correlated well with the experimental findings in the present study. The metal complexes showed appreciable antioxidant potential as predicted by the computational and experimental findings. The ligand possessed better NLO properties than urea.

© 2020 The Author(s). Published by Elsevier B.V. on behalf of King Saud University. This is an open access article under the CC BY-NC-ND license (<http://creativecommons.org/licenses/by-nc-nd/4.0/>).

## 1. Introduction

Through quantum mechanical simulations the structural characteristics of new materials can be easily and accurately predicted.

The computational predictions can also validate the experimental findings. Owing to the fast and accurate predictions by automated softwares, computational chemistry has received considerable attention (Matulkova et al., 2008; Boo et al., 2008). Due to the remarkable growth in the field of computational resources, many theoretical algorithms have been proposed to calculate various properties of a compound using semi-empirical and DFT methods. The theoretical data can be easily compared with the experimental one (Brewerton, 2008; Ravna and Sager, 2008). DFT has become a major tool for structure prediction and understanding the mechanistic approach (Lipkowitz et al., 2009; Lorenc et al., 2008). Quantum studies enable to envisage the structure of a chemical entity with the help of computer aided softwares. With the added

\* Corresponding author.

E-mail address: [tahminakhan30@yahoo.com](mailto:tahminakhan30@yahoo.com) (T. Khan).

Peer review under responsibility of King Saud University.



Production and hosting by Elsevier

<https://doi.org/10.1016/j.jksus.2020.101313>

1018-3647/© 2020 The Author(s). Published by Elsevier B.V. on behalf of King Saud University.

This is an open access article under the CC BY-NC-ND license (<http://creativecommons.org/licenses/by-nc-nd/4.0/>).

support of experimental results, new molecules of significant utility may be generated (Lorenc et al., 2008). Thiosemicarbazone are one such type of Schiff based ligands of known biological importance (Kola and Landis, 2004). Thiosemicarbazones have gained considerable interest owing to their binding ability with metal ions (Pelosi, 2010). They can bind to the metal ion *via* N and S atoms. The authors have reported the anticancer and antibacterial activity of (*E*)-2-(butan-2-ylidene)hydrazinecarbothioamide and its' complexes with Cu, Fe, Zn and Co salts in their previous manuscript where a significant activity enhancement was observed upon the coordination of metal ions (Khan et al., 2017). In this paper the experimental results obtained after the FT-IR, <sup>1</sup>H NMR, <sup>13</sup>C NMR and UV analysis have been verified by the quantum mechanics studies in this paper. The antioxidant activity of its' complexes has also been assessed using the DPPH assay. Molecular docking studies of the complexes were also performed against NADPH and MPO,

## 2. Materials and methods

For chemical synthesis, thiosemicarbazide, 2-butanone and ethanol were purchased from Fisher Scientific. <sup>1</sup>H and <sup>13</sup>C NMR spectra were recorded on a Bruker instrument on 500.1 MHz at 295 K using tetramethylsilane (TMS) as an internal standard. The sample was run in DMSO *d*<sub>6</sub>. Mass spectrum of the ligand was obtained on FAB-MS, JEOL SX-102 mass spectrometer. IR spectra were recorded on a Bruker vertex 70 IR spectrophotometer. UV spectrum was recorded on a SpectraMax-5 spectrophotometer (Molecular Devices) between 200 and 400 nm. Density functional methods were used to predict ligand's <sup>1</sup>H, <sup>13</sup>C, FT-IR and UV spectra. The DFT calculations have been carried out using Gaussian 09 software package with the internally stored DFT/B3LYP/6-31++G (d,p) basis set. NMR parameters were calculated using a single-point calculation through Guage independent atomic orbital (GIAO) approach and DFT/B3LYP method with 6-31++G(d,p) basis set and IEFPCM model with DMSO which was used to understand the solvent induced effect. The basis of selection was due to past studies showing good agreement between experimental and calculated chemical shifts (Fraser et al., 2013; White et al., 2015; Pierens et al., 2015). NMR parameters (NMR = GIAO) were calculated with a single-point calculation in gaseous and solvent phases both by the same basis set, using the optimized structures from the B3LYP/6-31++G(d,p) calculation. The structure was optimized in Gaussian 09 with the help of B3LYP/6-31++G(d,p) in vacuum. The characterization of the normal modes was done on the basis of the PED analysis using VEDA4 program and Gauss View 6.0 was used to visualize and analyze the normal modes. Molecular docking was performed using iGEMDOCK 2.1 and AutoDock 4.2.6. The target proteins NADPH-oxidase (PDB I.D.5VOH) and myeloperoxidase (MPO) (PDB I.D. 5FMA) were downloaded from www.rcsb.org/pdb.

## 3. Chemistry

### 3.1. Synthesis of 2-butanone thiosemicarbazone

The ligand was synthesized taking reference from a earlier published study with some alterations (Supplementary Fig. 1) (Khan et al., 2017; Kumar and Kumar, 2013).

#### 3.1.1. C<sub>5</sub>H<sub>11</sub>N<sub>3</sub>S

Yield: 90%, MW:145, Solubility: Ethanol, DMSO, DMF, MP(°C): 99 °C, FTIR (KBr) (cm<sup>-1</sup>): 1619 (C=N), 772, 1077 (C=S), <sup>1</sup>H NMR (DMSO) (ppm) 1.1 (t, 3H), 1.9 (s, 3H), 2.3 (q, 2H), 4.9 (s, 1H,NH), 7.69 (s, 2H,NH<sub>2</sub>), <sup>13</sup>C NMR (DMSO) (ppm): 10.70 (CH<sub>3</sub>), 18.72

(CH<sub>3</sub>), 31.62 (CH<sub>2</sub>), 155.5 (C=N) and 178.72 (C=S), ESI MS (*m/z*): 146.1 M<sup>+</sup>, λ<sub>max</sub> (nm): 267.

Four transition metal complexes of Cu, Fe, Zn and Co were prepared using the ligand with the chemical formulae [Cu(C<sub>5</sub>H<sub>11</sub>N<sub>3</sub>S)<sub>2</sub>(SO<sub>4</sub>)], [Fe(C<sub>5</sub>H<sub>11</sub>N<sub>3</sub>S)<sub>2</sub>(SO<sub>4</sub>)], [Zn(C<sub>5</sub>H<sub>11</sub>N<sub>3</sub>S)<sub>2</sub>(SO<sub>4</sub>)] and [Co(C<sub>5</sub>H<sub>11</sub>N<sub>3</sub>S)<sub>2</sub>Cl<sub>2</sub>]<sup>+</sup>. The detailed preparation and characterization of the complexes has already been described in our previous manuscript (Khan et al., 2017) and summarized in Supplementary Table 1.

## 4. Results and discussion

### 4.1. Spectral characterization of the ligand

The <sup>1</sup>H NMR spectrum of the ligand had signals due to CH<sub>3</sub>, CH<sub>2</sub>, NH and NH<sub>2</sub> groups. Significant shifting in values confirmed the formation of complexes. In the proton spectrum, a triplet at δ 1.1, singlet at δ 1.9, quartet at δ 2.3 were obtained corresponding to CH<sub>3</sub>, CH<sub>3</sub> and CH<sub>2</sub> groups respectively. Two small singlets at δ 4.9 and 7.69 were obtained for NH and NH<sub>2</sub> groups. The <sup>13</sup>C spectrum of the ligand revealed signals at δ 10.70, 18.72, 31.62, 155.5 and 178.72 corresponding to CH<sub>3</sub>, CH<sub>3</sub>, CH<sub>2</sub>, C=N and C=S groups. NH and NH<sub>2</sub> protons were most downfield. Mass spectrum of the ligand furnished a M<sup>+</sup> peak at 146 corresponding to its molecular weight of 145. The IR spectrum of the ligand showed a strong band at 1619 cm<sup>-1</sup> related to the azomethine group, ν(C=N) (Tada et al., 2011). The strong bands at 1077 cm<sup>-1</sup> & 772 cm<sup>-1</sup> were assigned to ν(C=S) (Bindu and Kurup, 1997). λ<sub>max</sub> of the ligand (267 nm) corresponded to π-π\* transition (Misner et al., 2003).

## 5. DFT analysis of the ligand

DFT is mainly used for theoretical calculations of electronic structure of a molecule. It is based on quantum mechanical semi-empirical approach for investigations. Theoretical observations may be useful for the prediction of interactions with biological macromolecules as well (Brewerton, 2008).

### 5.1. Frontier molecular orbital analysis

The energy gap between the highest occupied molecular orbital (HOMO) and the lowest occupied molecular orbital (LUMO) mainly governs the molecular electrical transport properties (Silverstein et al., 1981). HOMO denotes the nucleophilicity, whereas the

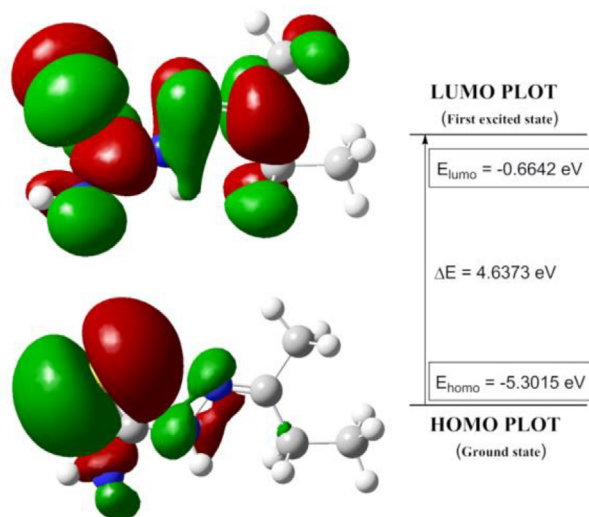


Fig. 1. HOMO-LUMO plot of ligand in isolated (gaseous) phase.

**Table 1**  
Selected optimized geometrical parameters of the ligand.

Bond length (Å)		Bond angle (°)		Dihedral angle (°)	
S1-C2	1.663	S1-C2-N3	126.0	S1-C2-N3-N4	-4.344
C2-N3	1.376	S1-C2-N9	122.4	C2-N3-N4-C5	173.109
N3-N4	1.364	C2-N3-N4	121.6	N3-N4-C5-C6	179.204
N4-C5	1.287	N3-N4-C5	118.2	N3-N4-C5-C7	-0.722
C5-C6	1.505	N4-C5-C6	115.5	N4-C5-C7-C8	-179.54
C5-C7	1.522	N4-C5-C7	123.8		
C7-C8	1.532	C5-C6-C8	116.3		
C2-C9	1.378				

LUMO represents the electrophilicity. They are also referred to as frontier molecular orbitals (FMOs). The HOMO and LUMO of the ligand is presented in Fig. 1. The negative value of the energy gap indicated molecular stability. Lower HOMO energy value indicated that the molecule has low electron donating ability (Barakat et al., 2015). The energy gap also predicts the intramolecular charge transfer (Padmaja et al., 2009).

HOMO-LUMO energy gap:

HOMO = -5.3015 eV

LUMO = -0.6642 eV

HOMO-LUMO energy difference = -4.6373 eV

### 5.2. Optimized geometry parameters

The main aim of geometry optimization is to find a new low energy conformation of the molecule. The geometry optimization was done by B3LYP/6-31++G(d,p) method. The N4-C5 bond length was 1.287 Å indicating double bond character (Table 1) (Mary et al., 2008). Bond lengths of S1-C2 and C2-C9 were 1.663 Å and 1.378 Å respectively indicating partial double bond character. Though the bond lengths were higher than that obtained for a pure double bond length (1.22 Å) suggesting multiple bond character (Politzer and Truhlar, 1981). The optimized structure of the ligand is presented as Supplementary Fig. 2.

### 5.3. Molecular electrostatic potential (MEP)

The electrophilic and nucleophilic sites on a molecule are predicted through MEP (Luque et al., 2000). The sites of negative potential are susceptible to nucleophilic attack whereas sites having positive potential are electrophilic. The positive electrostatic

potential is shown by blue colour and depicts the area of low electron density. This is the state of repulsion of the proton by the nucleus. The negative electrostatic potential depicted by red colour shows the attraction felt by the proton towards the electron density. Potential increases in the order red < orange < yellow < green < blue. MEP diagram of the ligand (Fig. 2) showed the presence of positive region around hydrogen atoms, whereas the negative region was found around sulphur atom associated with its lone pair.

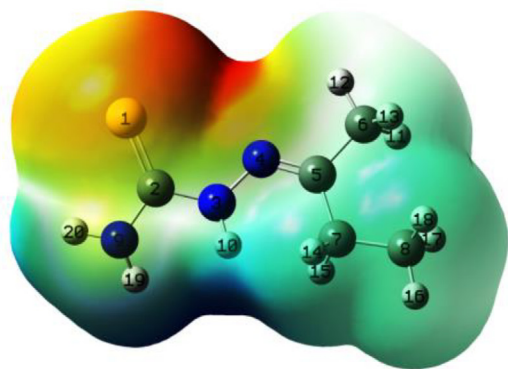
The color range, in kcal/mol, is: red greater than 4.5, 4.5 > yellow > -11.0, -11.0 > green > -26.6 and blue < -26.6.

### 5.4. NMR spectral analysis (<sup>1</sup>H NMR and FT-IR)

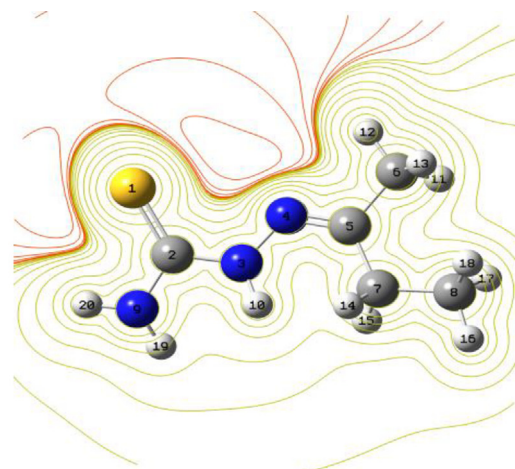
Experimental NMR spectrum of the ligand was obtained in DMSO. The calculated and experimental chemical shifts are given in Tables 2-3. The structure was optimized in Gaussian 09. The

**Table 2**  
Calculated and experimental <sup>1</sup>H NMR <sup>13</sup>C NMR chemical shifts (δ/ppm) in DMSO d<sub>6</sub> for ligand.

Atom	Exp. <sup>1</sup> H NMR	Calc. <sup>1</sup> H NMR	δ <sub>exp</sub> -δ <sub>cal</sub>
H-10	7.69	8.03	-0.34
H-19,20	4.82	4.74	0.08
H-11,12,13,	1.9	1.97	-0.07
H-14,15	2.3	2.00	0.3
H-16,17,18	1.1	1.03	0.07
Atom	Exp. <sup>13</sup> C NMR	Calc. <sup>13</sup> C NMR	δ <sub>exp</sub> -δ <sub>cal</sub>
C-2	178.72	180.98	-2.26
C-5	155.85	154.14	1.71
C-6	31.62	23.12	8.5
C-7	18.72	21.17	-2.45
C-8	10.70	8.70	2.0



(a)



(b)

**Fig. 2.** The MEP of Ligand, (a) 3D structure, (b) embedded 2D structure.

**Table 3**  
Experimental and calculated vibrational wave numbers ( $\text{cm}^{-1}$ ) of ligand.

Modes	IR <sub>Unscale</sub>	IR <sub>Scale</sub>	IR <sub>Observ</sub>	%PED
54	3689	3546	3448	[ $\nu$ as(N9H19)(72)- $\nu$ as(N9H20)(25)]
53	3547	3410	3371	[ $\nu$ s(N9H19)(72)- $\nu$ s(N9H20)(24)]
52	3532	3396	3251	[ $\nu$ (N3H10)(96)]
51	3163	3040	-	[ $\nu$ (C6H12)(88)]
50	3134	3012	-	[ $\nu$ as(C8H18)(50)- $\nu$ as(C8H17)(48)]
49	3127	3006	-	[ $\nu$ (C8H16)(64)- $\nu$ s(C8H17)(18)- $\nu$ s(C8H18)(17)]
48	3090	2970	2973	[ $\nu$ as(C6H13)(52)- $\nu$ as(C6H11)(47)]
47	3058	2940	2934	[ $\nu$ s(C8H16)(35)- $\nu$ s(C8H17)(32)- $\nu$ s(C8H18)(31)]
46	3039	2921	-	[ $\nu$ s(C6H11)(46)- $\nu$ s(C6H13)(40)- $\nu$ s(C6H12)(11)]
45	3018	2901	2906	[ $\nu$ as(C7H15)(50)- $\nu$ as(C7H14)(48)]
44	2991	2875	2886	[ $\nu$ s(C7H14)(51)- $\nu$ s(C7H15)(49)]
43	1702	1636	1619	[ $\nu$ (N4C5)(80)]
42	1640	1576	1572	[ $\nu$ ( $\sigma$ -H2ON9H19)(81)]
41	1558	1497	1502	[ $\nu$ ( $\sigma$ -H10N3N4)(66)- $\nu$ (N3C2)(12)]
40	1522	1463	-	[ $\nu$ ( $\sigma$ -H16C8H18)(44)- $\nu$ ( $\sigma$ -H18C8H17)(23)- $\nu$ ( $\delta$ -H18C8C7C5)(11)]
39	1520	1461	-	[ $\nu$ ( $\sigma$ -H17C8H16)(43)- $\nu$ ( $\sigma$ -H18C8H17)(25)- $\nu$ ( $\delta$ -H17C8C7C5)(11)]
38	1493	1435	1435	[ $\nu$ ( $\sigma$ -H13C6H12)(43)- $\nu$ ( $\sigma$ -H12C6H11)(19)- $\nu$ ( $\delta$ -H12C6C5C7)(13)]
37	1489	1432	-	[ $\nu$ ( $\sigma$ -H15C7H14)(40)- $\nu$ ( $\sigma$ -H11C6H13)(23)]
36	1484	1426	1420	[ $\nu$ ( $\sigma$ -H15C7H14)(30)- $\nu$ ( $\sigma$ -H11C6H13)(26)]
35	1435	1379	1386	[ $\nu$ ( $\omega$ -H17C8H16)(18)- $\nu$ ( $\omega$ -H16C8H18)(17)- $\nu$ ( $\omega$ -H18C8H17)(16)- $\nu$ ( $\omega$ -H11C6H13)(10)]
34	1433	1378	1368	[ $\nu$ (N3C2)(12)- $\nu$ ( $\omega$ -H16C8H18)(12)- $\nu$ ( $\omega$ -H17C8H16)(12)- $\nu$ ( $\omega$ -H18C8H17)(11)]
33	1409	1354	1349	[ $\nu$ (N3C2)(20)- $\nu$ ( $\sigma$ -H19N9C2)(16)- $\nu$ ( $\omega$ -H11C6H13)(11)]
32	1366	1313	1286	[ $\nu$ ( $\delta$ -H15C7C5C6)(28)- $\nu$ ( $\omega$ -H15C7H14)(17)- $\nu$ ( $\delta$ -H14C7C5C6)(16)]
31	1310	1259	1247	[ $\nu$ ( $\sigma$ -H14C7C8)(53)- $\nu$ ( $\gamma$ -H15C7C5C6)(19)- $\nu$ ( $\gamma$ -H14C7C5C6)(13)]
30	1307	1256	-	[ $\nu$ ( $\sigma$ -H10N3N4)(66)- $\nu$ (N9C2)(52)]
29	1280	1230	1221	[ $\nu$ (C6C5)(27)- $\nu$ (C7C5)(22)]
28	1179	1133	1107	[ $\nu$ (N3N4)(53)]
27	1121	1077	-	[ $\nu$ ( $\gamma$ -C8C7C5C6)(22)- $\nu$ ( $\gamma$ -H18C8C7C5)(13)]
26	1103	1060	1066	[ $\nu$ (C8C7)(27)- $\nu$ ( $\delta$ -H17C8C7C5)(13)- $\nu$ ( $\delta$ -H18C8C7C5)(12)]
25	1059	1018	1036	[ $\nu$ ( $\sigma$ -H19N9C2)(34)- $\nu$ (C8C7)(15)- $\nu$ (N3C2)(13)]
24	1025	985	995	[ $\nu$ ( $\delta$ -H13C6C5C7)(21)- $\nu$ ( $\delta$ -H11C6C5C7)(18)- $\nu$ (C8C7)(16)]
23	1018	979	981	[ $\nu$ ( $\gamma$ -H12C6C5C7)(30)- $\nu$ ( $\gamma$ -H14C7C8)(10)]
22	997	958	968	[ $\nu$ (C6C5)(13)- $\nu$ (C8C7)(20)- $\nu$ ( $\delta$ -H18C8C7C5)(18)- $\nu$ ( $\delta$ -H17C8C7C5)(16)]
21	796	765	772	[ $\nu$ (S1C2)(36)- $\nu$ (C7C5)(14)- $\nu$ ( $\sigma$ -C5N4N3)(11)]
20	793	762	-	[ $\nu$ ( $\gamma$ -H16C8C7C5)(22)- $\nu$ ( $\gamma$ -H14C7C5C6)(13)]
19	777	747	721	[ $\nu$ (C6C5)(23)- $\nu$ (C7C5)(28)- $\nu$ (S1C2)(14)]
18	640	615	-	[ $\nu$ ( $\gamma$ -S1N3N9C2)(71)]
17	590	567	583	[ $\nu$ (C6C5)(13)- $\nu$ ( $\sigma$ -C2N3N4)(13)- $\nu$ ( $\sigma$ -S1C2N9)(10)]
16	562	541	-	[ $\nu$ ( $\gamma$ -H2ON9C2N3)(32)- $\nu$ ( $\sigma$ -N9C2N3)(13)]
15	558	536	-	[ $\nu$ ( $\gamma$ -H2ON9C2N3)(45)- $\nu$ ( $\gamma$ -S1N3N9C2)(15)]
14	523	503	-	[ $\nu$ ( $\gamma$ -C7C6N4C5)(41)- $\nu$ ( $\gamma$ -H14C7C5C6)(15)]

 $\nu$  = Stretching. $\omega$  = Wagging. $\tau$  = Twisting. $\rho$  = Rocking. $\sigma$  = Scissoring. $\gamma$  = Out-of-plane deformation. $\delta$  = In-plane deformation.

experimental values were obtained between 1.1 and 7.69 ppm whereas the calculated values were between 1.03 and 8.03 ppm. The highest deviation was obtained for H14, 15 viz. 0.3 ppm. The  $^{13}\text{C}$  chemical shifts were obtained in the range 10.70–178.72 ppm experimentally. The theoretical values were between 8.70 and 180.98 ppm. The highest variation was for C6 viz. 8.5 ppm at the B3LYP level. A larger deviation is obtained for  $^{13}\text{C}$  chemical shifts than for  $^1\text{H}$ .  $^1\text{H}$  and  $^{13}\text{C}$  correlation coefficients ( $R^2$ ) were 0.9964 and 0.9974 respectively (Supplementary Fig. 3). A higher degree of correlation was obtained between  $^{13}\text{C}$  NMR experimental and calculated chemical shifts (Asadi et al., 2016).

### 5.5. Vibrational spectral analysis

The experimental and calculated (scaled as well as non-scaled) wave numbers were observed between 400 and 4000  $\text{cm}^{-1}$  and calculated PED are given in Table 3. The calculated and experimental IR spectra are given in Fig. 3. The correlation coefficient ( $R^2$ ) was 0.9984 showing good agreement

between the calculated and experimental values (Supplementary Fig. 4). The experimental and theoretical peak of C= was found at 1619 and 1639  $\text{cm}^{-1}$  respectively. The experimental and theoretical C=S peaks were obtained at 772 and 765  $\text{cm}^{-1}$  respectively (Roeges, 1994). The experimental and theoretical asymmetric  $\nu_{\text{as}}$  NH vibrations were obtained at 3448 and 3546  $\text{cm}^{-1}$  respectively. The experimental and theoretical symmetric  $\nu_{\text{sym}}$  vibrations were obtained at 3371 and 3410  $\text{cm}^{-1}$  respectively. The difference may be due to intermolecular interactions as the experimental spectrum was obtained in solid state. The stretching N-N vibration was at 1107  $\text{cm}^{-1}$  and the calculated value was 1133  $\text{cm}^{-1}$  (Singh et al., 2013; Gambino et al., 2007). The C-H in plane deforming vibration was observed at 1435  $\text{cm}^{-1}$  experimentally and coincided with the observed value. The difference between the experimental and calculated harmonic frequencies may be due to non competent treatment of electronic correlation (James et al., 2011). A scaling factor of 0.9613 was used to scale down the calculated wave number to remove any possible harmonicity (Pople et al., 1981).

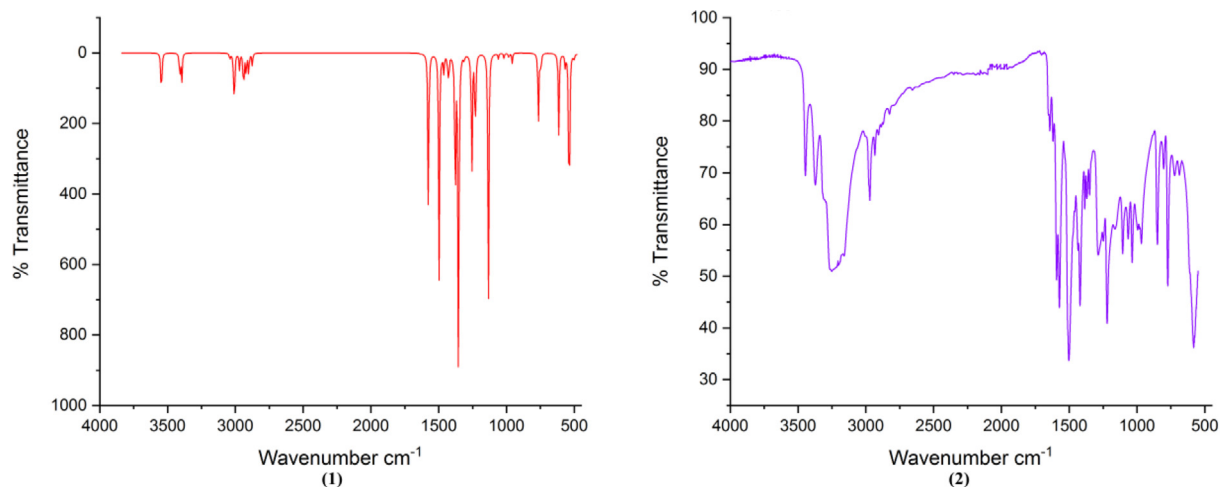


Fig. 3. Calculated (a) and Experimental (b) IR spectrum of ligand.

### 5.6. UV–vis spectral analysis

The UV–visible spectrum of 2-butanone thiosemicarbazone was calculated using the time dependent density functional theory (TD-DFT). The spectrum was obtained both in gaseous phase as well as in solvent phase in DMSO (Fig. 4). The experimental spectrum was recorded in DMSO with the  $\lambda_{max}$  obtained at 267 nm and a shoulder band (Khan et al., 2017). In gaseous phase three transitions at 303, 269 and 251 nm were obtained corresponding to  $\pi \rightarrow \pi^*$  charge

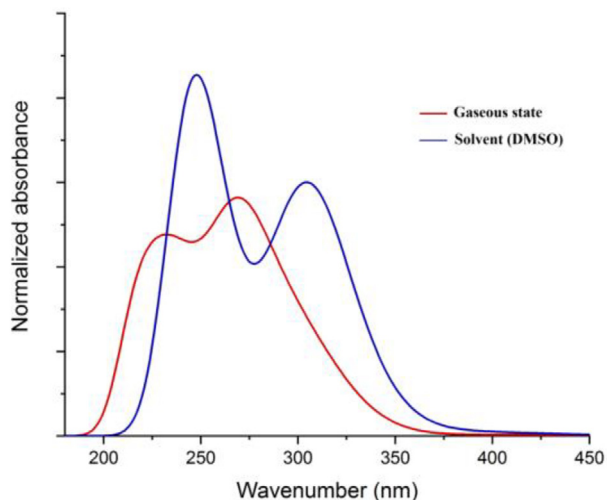


Fig. 4. TD-DFT predicted UV–vis spectra in gaseous and solvent (DMSO) states.

Table 4

TD-DFT calculated excitations in gaseous state and solvent (DMSO) states.

Excitation energy (eV)	Oscillator strength ( <i>f</i> )	Experimental wavelength (nm)	Calculated Wavelength (nm)	Major transition and expansion coefficient	Assignment	Contribution %
Gaseous state						
4.0873	0.0485	–	303.34	H(38) → L(40) (0.56614)	$\pi \rightarrow \pi^*$	32.05
4.6003	0.1208	–	269.51	H(39) → L(41) (0.57411)	$\pi \rightarrow \pi^*$	32.96
4.9298	0.0025	–	251.50	H(38) → L(41) (0.63928)	$\pi \rightarrow \pi^*$	40.86
Solvent (DMSO)						
4.0579	0.1455	–	305.54	H(38) → L(40) (0.64965)	$\pi \rightarrow \pi^*$	42.20
4.7421	0.0378	267	261.45	H(39) → L(41) (0.53050)	$\pi \rightarrow \pi^*$	28.14
4.9970	0.1022	–	248.12	H(37) → L(40) (0.53544)	$\pi \rightarrow \pi^*$	28.66

transfer transition. The  $\pi \rightarrow \pi^*$  transition is mainly governed by HOMO → LUMO excitation. In solvent phase (DMSO) transitions at 305, 261 and 248 nm were obtained. The electronic transitions are presented in Table 4. Transitions involved with oscillator strength viz.  $f = 0.1455$  and  $0.1022$  were not obtained experimentally. The electronic transitions were accompanied by a slight red shift in DMSO which may be attributed to electrostatic and dispersion contributions and H-bonding (Krawczyk, 2015). Solvatochromic changes also occur when polarity of the medium is changed (Zakerhamidi et al., 2012).

### 5.7. Global reactivity descriptors

Hardness ( $\eta$ ), global softness (*S*), electronegativity ( $\chi$ ), chemical potential ( $\mu$ ) and electrophilicity index ( $\omega$ ) are the global reactivity descriptors generally used to predict the stability and reactivity (Geerlings et al., 2003). The electrophilicity index describes the tendency of a molecule to accept electron. A nucleophile has a lower value of  $\omega$ , whereas an electrophile has high value of  $\omega$  (Babu and Jayaprakash, 2015). The value of chemical potential ( $\mu$ ) describes the reactivity of the compound. The greater the electronic potential, more reactive would be the compound. According to Koopman's theorem, global reactivity descriptors are calculated using HOMO and LUMO of the FMOs (Parr and Yang, 1989). The low value of global electrophilicity index (1.9185) indicated ligand's nucleophilic nature. The ionization energy (*I*) and electron affinity (*A*) can be predicted through HOMO and LUMO orbital energies as  $I = -E_H$  and  $A = E_L$ .  $\Delta N_{max}$  defines the electrophilic charge transfer (ECT) between the two molecules. If ECT is greater than 0 then charge flows from second molecule to first. ECT is calculated from the equation-  $ECT = (\Delta N_{max})_1 -$

$(\Delta N_{\max})_2$ , here  $(\Delta N_{\max})_1 = -(\mu/\eta)_1$  and  $(\Delta N_{\max})_2 = -(\mu/\eta)_2$ . The  $\Delta N_{\max}$  for the reacting molecules is 1.2868 indicating that the charge flows from molecule 2 to 1 (Singh and Singh, 2015). Calculated global descriptors are given in Supplementary Table 2.

### 5.8. Natural bond orbital analysis (NBO)

NBO also helps in understanding the hybridization, covalent bonding, hydrogen bonding and van der Waals interaction (Glendening et al., 2001). Second order perturbation theory analysis of the Fock matrix in the NBO basis for intermolecular interactions was calculated by DFT/B3LYP/6-311++G(d,p) method is presented in Supplementary Table 3. Stable donor to acceptor interactions involve delocalization of electron density between occupied Lewis-type (bonding or lone pair) NBO's and unoccupied (antibonding) non-Lewis NBO's (Glendening et al., 2001). The most important interaction was related to electron donation from  $n(2)S1$  atom to the  $\sigma^*C2-N3$  resulting in the maximum stabilization energy 19.08 kcal/mol.

### 5.9. Thermodynamic calculations

Thermodynamic energies were calculated using vibrational frequency calculations for the ligand at 298.15 K. The values of enthalpy ( $\Delta H_{\text{Reaction}}$ ), Gibbs free energy ( $\Delta G_{\text{Reaction}}$ ) and entropy change of reaction ( $\Delta S_{\text{Reaction}}$ ) are given in Supplementary Table 4. The negative values of  $\Delta H$  and  $\Delta G$  indicated that the ligand formation is exothermic and spontaneous at room temperature. The free energy of the molecule was calculated including the zero-point vibrational energy.

#### 5.9.1. Non-linear optical properties

To test the non-linear optical response of the ligand, dipole moment ( $\mu_0$ ), polarizability ( $\alpha_0$ ), anisotropy of polarizability ( $\Delta\alpha$ ) and first hyperpolarizability ( $\beta_0$ ) were calculated at B3LYP/6-31++G(d,p) basis set level.

The calculated polarizability of the ligand ( $\Delta\alpha$ ) was  $6.1054 \times 10^{-23}$  esu and  $\alpha_0$  and  $\beta_0$  were  $1.3533 \times 10^{-23}$  esu and  $4.8098 \times 10^{-30}$  esu respectively. Urea is one of the archetypal compounds known for its NLO properties (Supplementary Table 5). The  $\beta_0$  value of urea is  $0.13 \times 10^{-30}$  esu. The hyperpolarizability of the ligand was higher than urea.

## 6. Molecular docking studies

iGEMDOCK 2.1 is a graphical, automated software for integrated docking. For docking, protein and ligand structure files were prepared. The binding sites were defined and prepared. The set parameters were as follows: screening: population size = 800, generations = 80, number of solutions = 10. The empirical scoring function of iGEMDOCK is estimated as:

$$\text{Fitness} = \text{vdW} + \text{H bond} + \text{Elec}$$

where, vdW = van der Waal energy, H bond = hydrogen bonding energy, Elec = electrostatic energy

The ligand was docked with the binding site using accurate docking function (slow docking). AutoDock 4.2.6 was also used for the prediction of the binding energy. Ligand and its four complexes were docked with NADPH oxidase and MPO. Many cellular pathways and environmental conditions cause production of reactive oxygen species (ROS) (Singh and Singh, 2015). Reactive oxygen and nitrogen species are often produced by cellular enzymes such as myeloperoxidase, cytochrome P450 oxidases and NADPH oxidases (Singh and Singh, 2015) etc. Energy minimization was done by General AMBER force field (GAFF). Against NADPH [ $\text{Fe}(\text{C}_5\text{H}_{11}\text{N}_3\text{S}_2)\text{SO}_4$ ] possessed minimum energy viz.  $-105.60$  kcal/mol and  $-6.9$  kcal/mol. Against MPO also [ $\text{Fe}(\text{C}_5\text{H}_{11}\text{N}_3\text{S}_2)\text{SO}_4$ ] showed minimum binding energies  $-116$  and  $-7.3$  kcal/mol as predicted by the two softwares. The docking poses of Fe complex are shown as Fig. 5 (a,b). Docking interactions are given in (Supplementary Tables 6–7 and Fig. 5–6).

### 6.1. Free radical scavenging activity

The free radical scavenging activity of all the synthesized metal complexes was evaluated by DPPH Assay (Scherer and Godoy, 2009). The antioxidant activity was tested at 10, 50, 80 and 100  $\mu\text{M}$  concentration. The absorbance was measured at 517 nm. Lower the absorbance, higher would be the free radical scavenging activity. The scavenging the DPPH radical was calculated by using the following formula:

$$\text{DPPH scavenging effect (\% inhibition)} = [(A_c - A_s)/A_c] \times 100$$

where,  $A_c$  = absorbance of the control reaction (DPPH solution) and  $A_s$  = absorbance of the complexes

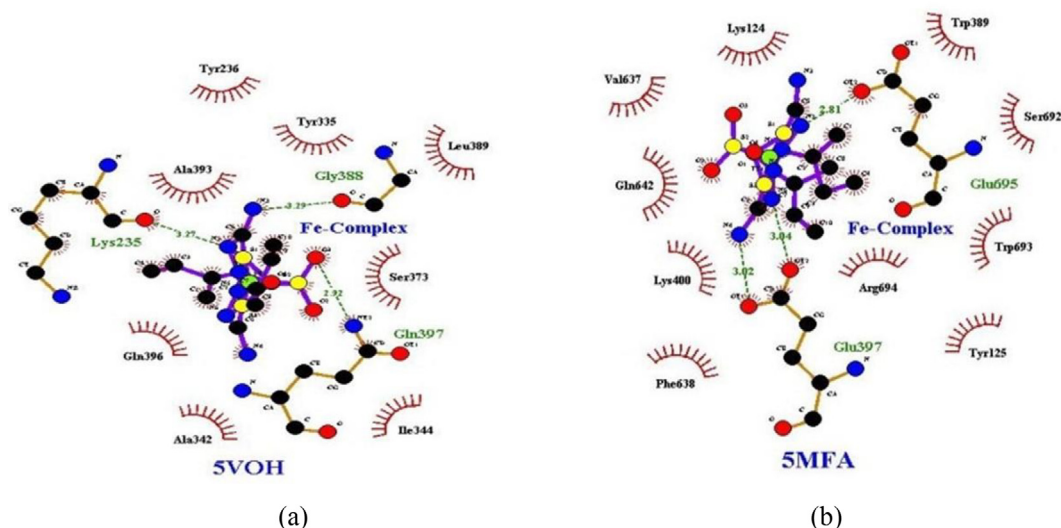


Fig. 5. Docking poses of [ $\text{Fe}(\text{C}_5\text{H}_{11}\text{N}_3\text{S}_2)(\text{SO}_4)$ ] with (a) NADPH and (b) MPO.

**Table 5**  
Percentage scavenging ability of complexes.

Complex	10 $\mu$ M/mL	50 $\mu$ M/mL	80 $\mu$ M/mL	100 $\mu$ M/mL
[Cu(C <sub>5</sub> H <sub>11</sub> N <sub>3</sub> S) <sub>2</sub> SO <sub>4</sub> ]	67.55	68.13	68.13	72.61
[Fe(C <sub>5</sub> H <sub>11</sub> N <sub>3</sub> S) <sub>2</sub> SO <sub>4</sub> ]	72.61	73.16	77.80	81.70
[Zn(C <sub>5</sub> H <sub>11</sub> N <sub>3</sub> S) <sub>2</sub> SO <sub>4</sub> ]	64.43	64.89	64.89	73.55
[Co(C <sub>5</sub> H <sub>11</sub> N <sub>3</sub> S) <sub>2</sub> Cl <sub>2</sub> ] <sup>+</sup>	67.85	70.04	74.60	77.15

Uncontrolled generation of ROS causes redox imbalance and oxidative stress harmful for many diseases including cancer and neurological disorders. The antioxidant activity is summarized in Table 5. [Fe(C<sub>5</sub>H<sub>11</sub>N<sub>3</sub>S)<sub>2</sub>(SO<sub>4</sub>)] showed maximum antioxidant activity viz. 81.70% followed by [Co(C<sub>5</sub>H<sub>11</sub>N<sub>3</sub>S)<sub>2</sub>Cl<sub>2</sub>]<sup>+</sup> (77.15%).

## 7. Future scope of the study

The study has elaborated the use of DFT technique for the prediction of molecular structure and prediction of important properties of the compound. The potential NLO properties of the ligand may be explored further for its use in optical devices. Furthermore, the potential antioxidant activity of the complexes can also be useful for the development of antioxidant drugs.

## 8. Conclusion

2-butanone thiosemicarbazone was synthesized and characterized by <sup>1</sup>H and <sup>13</sup>C NMR, FT-IR, UV-Vis and mass spectroscopic techniques. The experimental data was validated using DFT generated theoretical data. DFT analysis mainly correlates electronic structure of compound long with various parameters such as HOMO-LUMO, MEP, spectral as well as chemical reactivity analysis. It also explains internal hydrogen bonding along with other interactions. On the other hand, docking analysis provides information about the interaction of a lead compound with the target proteins. HOMO-LUMO energy gap illustrates the chemical stability which is an important decisive factor for the prediction of the reactivity of a molecule. The FMO analysis predicted that the molecule is stable. The low value of global electrophilicity index (1.9185) indicated its nucleophilic nature. In solvent phase the  $\lambda_{\max}$  values experienced a slight red shift. In case of NMR, a larger deviation was obtained for <sup>13</sup>C chemical shifts than for <sup>1</sup>H. The antioxidant activity of four complexes of the ligand was tested using DPPH assay. Fe complex was found to possess maximum antioxidant potential followed by Cu complex. Molecular docking studies showed that the Fe complex released the minimum binding energy. The docking results were further validated by the experimental results of the antioxidant activity.

## Acknowledgements

The authors are thankful to Mr. Mohsin Ali Khan, Chancellor, Era's University, Lucknow, for extending the necessary facilities and co-operation for carrying out *in silico* studies and biological activity evaluation. The authors are also thankful to the R&D wing of Integral University, Lucknow, for allotting the communication number (IU/R&D/2018-MCN000260) to the manuscript. Dr. Mohammad Azam is thankful to the support through Researchers Supporting Project number (RSP-2020/147), King Saud University, Riyadh, Saudi Arabia.

## Declaration of Competing Interest

The authors declare that they have no known competing financial interests or personal relationships that could have appeared to influence the work reported in this paper.

## Funding

This research did not receive any specific grant from any specific grant from funding agencies in the public, commercial, or not-for-profit sectors.

## Appendix A. Supplementary data

Supplementary data to this article can be found online at <https://doi.org/10.1016/j.jksus.2020.101313>.

## References

- Matulkova, L., Nemeš, I., Teubner, K., Nemeš, P., Mická, Z.J., 2008. Novel compounds of 4-amino-1, 4-triazole with dicarboxylic acids—crystal structures, vibrational spectra and non-linear optical properties. *J. Mol. Struct.* 873, 46–60.
- Boo, B.H., Lee, J.K., Lim, E.C., 2008. Ab initio, DFT, and spectroscopic studies of excited-state structure and dynamics of 9-ethylfluorene. *J. Mol. Struct.* 892, 110–115. <https://doi.org/10.1016/j.molstruc.2008.05.004>.
- Brewerton, S.C., 2008. The use of protein–ligand interaction fingerprints in docking. *Curr. Opin. Drug Discov. Devel.* 11, 356–364.
- Ravna, A.W., Sager, G., 2008. Molecular model of the outward facing state of the human multidrug resistance protein 4 (MRP4/ABCC4). *Bioorg. Med. Chem. Lett.* 18, 3481–3483.
- Lipkowitz, K.B., Cundari, T.R., Boyd, D.B., 2009. *Reviews in Computational Chemistry*. John Wiley & Sons.
- Lorenc, J., Bryndal, I., Marchewka, M.K., Kucharska, E., Lis, T., Hanuza, J., 2008. Crystal and molecular structure of 2-amino-5-chloropyridinium hydrogen selenite and its IR and Raman spectra, DFT calculations and physicochemical properties. *J. Raman Spectrosc.* 39, 863–872.
- Kola, I., Landis, J., 2004. Can the pharmaceutical industry reduce attrition rates? *Nature Reviews and Drug Dis.* 3, 711–715.
- Pelosi, G., 2010. Thiosemicarbazone metal complexes: from structure to activity. *Open Crystal J.* 3, 16–28.
- Khan, T., Dixit, S., Ahmad, R., Raza, S., Azad, I., Joshi, S., Khan, A.R., 2017. Molecular docking, PASS analysis, bioactivity score prediction, synthesis, characterization and biological activity evaluation of a functionalized 2-butanone thiosemicarbazone ligand and its complexes. *J. Chem. Biol.* 10, 91–104.
- Fraser, J.A., Lambert, L.K., Pierens, G.K., Bernhardt, P.V., Garson, M.J., 2013. Secondary metabolites of the sponge-derived fungus *Acremonium persicinum*. *J. Nat. Prod.* 76.
- White, A.M., Pierens, G.K., Forster, L.C., 2015. Rearranged diterpenes and norditerpenes from three Australian *Goniobranchus* mollusks. *J. Nat. Prod.* 79, 477–483.
- Pierens, G.K., Venkatachalam, T., Reutens, D.C., 2015. Comparison of experimental and DFT-calculated NMR chemical shifts of 2-amino and 2-hydroxyl substituted phenyl benzimidazoles, benzoxazoles and benzothiazoles in four solvents using the IEF-PCM solvation model. *Magn. Reson. Chem.* 54, 298–307.
- Kumar, S., Kumar, N., 2013. Synthesis, characterization and antimicrobial studies on some transition metal complexes of thiosemicarbazone. *Int. J. Res. Pharm. and Bio. Sci.* 4, 305–311.
- Tada, R., Chavda, N., Shah, M.K., 2011. Synthesis and characterization of some new thiosemicarbazide derivatives and their transition metal complexes. *J. Chem. Pharm. Res.* 3, 290–297.
- Bindu, P., Kurup, M.R.P., 1997. E.S.R. and electrochemical studies of four- and five-coordinate copper(II) complexes containing mixed ligands. *Trans. Met. Chem.* 22, 578–582.
- Misner, M.J., Skaff, H., Emrick, T., Russell, T.P., 2003. Directed Deposition of Nanoparticles Using Diblock Copolymer Templates. *Adv. Mat.* 15, 221–224. <https://doi.org/10.1002/adma.200390050>.
- Silverstein, R.M., Bassler, G.C., Morrill, T.C., 1981. *Spectrometric Identification of Organic Compounds*. Wiley, New York.
- Barakat, A., Al-Najjar, H.J., Al-Majid, A.M., Soliman, S.M., Mabkhot, Y.N., Shaik, M.R., Ghabbour, H.A., Fun, H.K., 2015. Synthesis, NMR, FT-IR, X-ray structural characterization, DFT analysis and isomerism aspects of 5-(2,6-dichlorobenzylidene)pyrimidine-2,4,6-(1H,3H,5H)-trione. *Spectrochim Acta A: Mol. Bio. Spect.* 147, 107–116. <https://doi.org/10.1016/j.saa.2015.03.016>.
- Padmaja, L., Ravi, K.C., Sajan, D., Joe, I.H., Jayakumar, V.S., Pettit, G.R., Nielsen, O.F., 2009. Density functional study on the structural conformations and intramolecular charge transfer from the vibrational spectra of the anticancer drug combretastatin-A2. *J. Raman Spectrosc.* 40, 419–428.
- Mary, Y.S., Varghese, H.T., Panicker, C.Y., Ertan, T., Yildiz, I., Temiz-Arpaç, O., 2008. Vibrational spectroscopic studies and ab initio calculations of 5-nitro-2-(p-fluorophenyl)benzoxazole. *Spectrochim. Acta.* 71A, 566–571. <https://doi.org/10.1016/j.saa.2007.12.041>.
- Politzer, P., Truhlar, D.G. (Eds.), 1981. *Chemical Application of Atomic and Molecular Electrostatic Potentials*. Plenum, New York.
- Luque, F.J., Lopez, J.M., Orozco, M., 2000. Perspective on Electrostatic interactions of a solute with a continuum. A direct utilization of ab initio molecular potentials for the prevision of solvent effects. *Theor. Chem. Acc.* 103, 343–345.

- Asadi, Z., Esrafil, M.D., Vessally, E., Asnaashariisfahani, M., Yahyaei, S., Khani, A., 2016. A structural study of fentanyl by DFT calculations, NMR and IR spectroscopy. *J. Mol. Str.* 1128, 552–562.
- Roeges, N.P.G., 1994. *A Guide to the Complete Interpretation of Infrared Spectra of Organic Structures*. Wiley, New York.
- Singh, R.N., Kumar, A., Tiwari, R.K., Rawat, P., 2013. A combined experimental and theoretical (DFT and AIM) studies on synthesis, molecular structure, spectroscopic properties and multiple interactions analysis in a novel Ethyl-4-[2-(thiocarbamoyl)hydrazinylidene]-3,5-dimethyl-1H-pyrrole-2-carboxylate and its dimer. *Spectrochim. Acta Part A Mol. Biomol. Spectrosc.* 112, 182–190. <https://doi.org/10.1016/j.saa.2013.04.002>.
- Gambino, D., Otero, L., Vieites, M., Boiani, M., Gonzalez, M., Baran, E.J., Cerecetto, H., 2007. Vibrational spectra of palladium 5-nitrofuryl thiosemicarbazone complexes: Experimental and theoretical study, *Spectrochim. Acta Part A Mol. Biomol. Spectrosc.* 68, 341–348. <https://doi.org/10.1016/j.saa.2006.11.043>.
- James III, W.H., Buchanan, E.G., Müller, C.W., Dean, J.C., Kosenkov, D., Slipchenko, L. V., Guo, L., Reidenbach, A.G., Gellman, S.H., Zwier, T.S., 2011. Evolution of amide stacking in larger  $\gamma$ -peptides: triamide H-bonded cycles. *J. Phys. Chem. A* 115, 13783–13798.
- Pople, J.A., Schlegel, H.B., Krishnan, R., Defrees, D.J., Binkley, J.S., Frisch, M.J., Whiteside, R.A., Hout, R.F., Hehre, W.J., 1981. Molecular orbital studies of vibrational frequencies. *Int. J. Quantum Chem.* 15, 269–278.
- Krawczyk, P., 2015. Time-dependent density functional theory calculations of the solvatochromism of some azo sulfonamide fluorochromes. *J. Mol. Model.* 21, 118.
- Zakerhamidi, M.S., Ahmadi-Kandjan, S., Moghadam, M., Ortyl, E., Kucharski, S., 2012. Solvatochromism effects on the dipole moments and photo-physical behavior of some azo sulfonamide dyes. *Spectro Acta Part A* 85, 105–110.
- Geerlings, P. De, Proft, F., Langenaeker, W., 2003. Conceptual density functional theory. *Chem. Rev.* 103, 1793–1874.
- Babu, N.S., Jayaprakash, D., 2015. Global and reactivity descriptors studies of cyanuric acid tautomers in different solvents by using of density functional theory (DFT). *J. Chem. Pharm. Res.* 7, 1155–1160.
- Parr, R.G., Yang, W., 1989. *Density Functional Theory of Atoms and Molecules*. Oxford University Press, Oxford, New York.
- Singh, R.K., Singh, A.K., 2015. Synthesis, molecular structure, spectral analysis, natural bond order and intramolecular interactions of 2-acetylpyridine thiosemicarbazone: A combined DFT and AIM approach. *J. Mol. Str.* 1094, 61–72.
- Glendening, E.D., Reed, A.E., Carpenter, J.E., Weinhold, F., 2001. *NBO Version 3.1*. Gaussian Inc., Pittsburgh, PA.
- Singh, A.K., Singh, R.K., 2015. Synthesis, crystal structure, spectroscopic analysis and computational study of (Z)-1-(2, 4-dinitrophenyl)-2-((E)-3-(4-methoxyphenyl)-1-(thiophen-2-yl) allylidene) hydrazine by DFT and AIM approach. *J. Mol. Str.* 1089, 191–205. <https://doi.org/10.1016/j.molstruc.2015.02.029>.
- Scherer, R., Godoy, H.T., 2009. Antioxidant activity index (AAI) by the 2,2-diphenyl-1-picrylhydrazyl method. *Food Chem.* 112, 654–658. <https://doi.org/10.1016/j.foodchem.2008.06.026>.